

Analytical Method for an FSS-Sandwiched Dual-Band Reflectarray Antenna

Baokun Xi^{1, 2}, Qianzhong Xue^{1, 2, *}, Yang Cai³, Lan Bi^{1, 2}, and Yong Wang^{1, 2}

Abstract—This paper presents an analytical method for designing a high-efficiency frequency selective surface FSS-sandwiched dual-band circularly polarized reflectarray antenna. Results are obtained using Computer Simulation Technology Microwave Studio (CST MWS). The antenna is designed to operate within the receiving (19.6–21.2 GHz) and transmitting (29.4–31 GHz) bands while sharing the same unit and aperture. A double-layer FSS is loaded between the upper and lower antennas to suppress mutual coupling. An analytical approximation method using conformal mapping to determine the effective permittivity ($\epsilon_{r,eff}$) is observed. The transmission and reflection coefficients of the proposed FSS are synthesized using the transmission line approach. The comprehensive analyzed results obtained are compared with results obtained from simulations performed in CST MWS. To validate the performance of the proposed FSS-backed element configuration, a 20/30-GHz dual-band circularly polarized reflectarray with a 90-mm aperture is designed. The simulated gains are 23.3 dBi at 20 GHz and 27.7 dBi at 30 GHz with aperture efficiencies exceeding 47.25% and 57.85% in the receiving and transmitting bands, respectively.

1. INTRODUCTION

Low complexity, low fabrication cost, and small physical size are crucial factors for antenna viability in satellite communications [1]. Reflectarray antennas (RAs) offer promising opportunities for wireless satellite communications links compared with conventional parabolic reflectors. Ka bands with circular polarization links can provide broad bandwidth for high-speed services [2]. It is necessary to design an antenna that can cover the two-frequency band of both the Ka-band downlink and Ka-band uplink. In this paper a dual-band reflectarray is introduced to cover both the downlink frequency band for receiving from 19.6 to 21.2 GHz and the uplink frequency band for transmitting from 29.5 to 31 GHz.

A single-layer Ka-band and dual-band reflectarray is demonstrated in [3]. The reflectarray uses a concentric dual split-loop to adjust the phase in two bands. However, the mutual coupling in a single layer seriously affects the bandwidth and efficiency performance. An efficient technique for reducing the mutual coupling in a multiband reflectarray involves replacing the ground plane with a frequency selective surface (FSS). At the cost of a complex structure, it is desirable to further suppress the mutual coupling and improve the antenna efficiency and bandwidth. A variety of cell elements are presented in [4] for the construction of an FSS-backed reflectarray. It is found that an FSS composed of open rings is the best candidate for the FSS-backed reflectarray due to its superior phase and amplitude response within the bandwidth. A multiband X/Ka-band reflectarray is demonstrated in [5], in which the Ka-band reflectarray is located on top of the X-band reflectarray to design a multiband X/Ka-band reflectarray. A dual-band reflectarray with mutual coupling effectively suppressed by using FSS

Received 25 July 2018, Accepted 23 October 2018, Scheduled 18 December 2018

* Corresponding author: Qianzhong Xue (qianzhong_xue@mail.ie.ac.cn).

¹ Key Laboratory of High Power Microwave Sources and Technologies, Institute of Electronics, Chinese Academy of Sciences, Beijing 100190, China. ² University of Chinese Academy of Sciences, Beijing 100049, China. ³ Space Engineering University, Beijing 100049, China.

with double-layer double concentric square loops is reported in [6]. However, to obtain a flat response in the desired band and a sharp decrease in the unwanted band, the numerical full-wave simulation optimization of the multilayer FSS often requires an enormous amount of computing resources.

Conformal mapping is the process of transforming a given coordinate system into a different coordinate system that preserves the angles between the vertices of the two coordinate systems [7]. In the field of high-speed electronics, the capacitance of transmission line structures on printed circuit boards (PCBs) is often approximated using conformal mapping techniques. To determine the capacitance in a PCB transmission line system, a conformal map that transforms a cross section of the strip-line geometry into two infinite parallel plates may be used [8].

In this study, a stacked reflectarray configuration with an aperture shared by both frequency bands is investigated, and a theoretical analysis of this FSS-backed reflectarray antenna is performed. Conformal mapping is used to analyze the S -parameter of the FSS. Analytical calculations of the response of the FSS in the presence of dielectrics can facilitate the initial FSS design and analysis prior to the use of full-wave simulation in more detailed studies. This design approach reduces the need for computationally intensive full-wave simulation-based design optimization; instead, it uses only full-wave simulation for more robust and detailed verification of the final FSS design. The transmission and reflection coefficients can be calculated analytically. This cascade configuration is composed of two arrays: a single-layer conventional 20-GHz band array and a double-layer FSS-backed 30-GHz band array. The mutual coupling between the two proposed frequency bands is suppressed by the multilayer FSS.

2. CONFIGURATION OF THE PROPOSED ANTENNA

Figure 1 shows a schematic of the proposed dual-band reflectarray. As observed from the feed side, the higher operating band reflectarray should precede the ones with a lower operating band. Grating lobes may be excited at the higher band if the sequence is reversed. A full-wave CST simulation with periodic boundary conditions is performed. The elements of the reflectarray are selected based on their own bands of operation and then set into the same periodic lattice configuration on separate layers. The higher-band reflectarray consisting of double-ring loops with different sizes is etched onto an FSS-sandwiched substrate. Considering the need to enhance the bandwidth of the whole structure, a bilayer FSS unit is adopted. The S -parameter of cascading FSS can change gently in the band and more steeply out of the band. A two-layer single-square-loop unit is used as the FSS element to provide more degrees of freedom for optimization. The FSS is designed to have a maximum reflection magnitude at 30 GHz and a maximum transmission coefficient (minimum reflection loss) at 20 GHz. Thus the FSS is designed to serve as a ground plane for the upper elements. The wide range of phase values is realized by variations in the size of the double-ring loops printed on the surface of the bottom substrate; the FSS parameters are left intact. Because of the simplicity of the structure, the proposed unit has the same structure for both bands with the same lattice size, $P = 4.5$ mm, namely, $0.3\lambda_d$ at 20 GHz and $0.45\lambda_u$ at 30 GHz, where λ_d and λ_u are the wavelengths of the center frequencies of the downlink and uplink bands, respectively. The element is specifically designed to contain three Taconic TLY substrate layers ($\epsilon_r = 2.2$, loss tangent = 0.0009), and the parameters are set to $h_1 = h_3 = h_5 = 0.508$ mm and $h_2 = h_4 = 2$ mm.

3. ANALYSIS OF THE FSS USING CONFORMAL MAPPING

By adding FSS as a band separator, the antenna could be designed to provide a full-phase shift range over the reflectarray aperture in the two different frequency bands. As the first design step, the FSS structure should be designed to control the incident wave and isolate the mutual coupling between the two resonance regions. For simplicity, we choose a square loop as the FSS. The frequency response of the FSS to incident radiation is shown in Fig. 4(b). The frequency response of the FSS to incident radiation is commonly calculated in MATLAB using an equivalent LC circuit model. However, the dielectric material alters the capacitive couplings among the elements of the FSS, and we use the equivalent permittivity of the substrate to scale the wavelength in the FSS's inductance/capacitance approximation equations. Hence the revised LC circuit model is obtained. The independent inductance

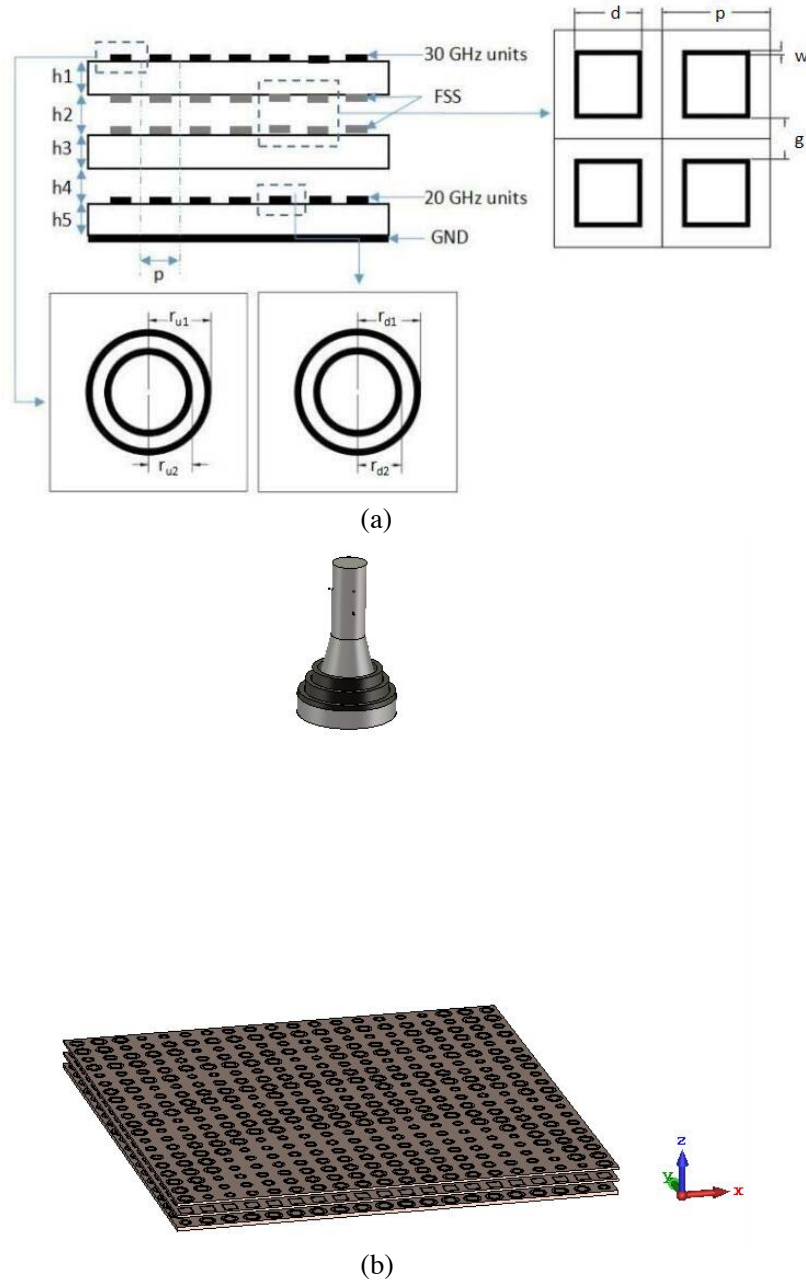


Figure 1. (a) Side view of the proposed antenna. (b) Schematic of the proposed antenna.

and capacitance of the FSS must be calculated in the absence of dielectrics to determine the freestanding impedance of the FSS. This calculation can be accomplished using the modified Marcuvitz strip grating equations [9]. The shape and dimensions of the FSS element play the most significant role in determining the frequency response of the FSS. The dimensions of the loop FSS are the conductor’s length (d) and width (w), the gap width (g), and the element length (p , which is equal to $d + g$). The inductive reactance, X , is calculated as $X = \frac{d}{p}F(p, 2s, \lambda)$, which corresponds to an inductance given as L . Next, the susceptance, B , which corresponds to the capacitance given by C , is calculated as $B = 4\frac{d}{p}F(p, g, \lambda)$. The variables are described by the following equations [9].

$$F(p, w, \lambda) = \frac{p \cos \theta}{\lambda} \left[\ln \csc \left(\frac{\pi w}{2p} \right) + G(p, w, \lambda, \theta) \right] \quad (1)$$

$$G(p, x, \lambda, \theta) = \frac{1}{2} \frac{(1 - \beta^2)^2 \left[\left(1 - \frac{\beta^4}{4}\right) (A_+ + A_-) + 4\beta^2 A_+ A_- \right]}{\left(1 - \frac{\beta^4}{4}\right) + \beta^2 \left(1 + \frac{\beta^2}{2} - \frac{\beta^4}{4}\right) (A_+ + A_-) + 2\beta^6 A_+ A_-} \quad (2)$$

$$A_{\pm} = \frac{1}{\sqrt{1 \pm \frac{2p \sin(\theta)}{\lambda} - \left(\frac{p \cos(\theta)}{\lambda}\right)^2}} - 1 \quad (3)$$

$$\beta = \sin\left(\frac{\pi w}{wp}\right) \quad (4)$$

After computing the impedance of the FSS, the S -parameter can be found by employing MATLAB, as shown in Fig. 4(b). The frequency response does not match well with the simulation in CST, which means that the dielectric material alters the capacitive couplings among the elements of the FSS. When a surrounding dielectric is sufficiently thick (relative to the wavelength), the resonant frequency of the FSS changes. As such, analytical methods are needed to determine the FSS's response to cascading.

To illustrate the application of conformal mapping in this design, Fig. 2(a) shows the electric field distribution between adjacent elements of the FSS. When the incident wave is polarized parallel to two segments in the loop, surface currents are excited in the direction of polarization of the incident wave. Because the majority of the coupling occurs between parallel conductor segments, the capacitance of this structure can be assumed to be equivalent to that of two coplanar strips. In [8], the characteristics of coplanar transmission lines on multilayer substrates can be expressed by analytic formulas obtained using conformal mapping. The capacitance of this FSS is assumed to be equivalent to the capacitance of the coplanar transmission line geometry. While this assumption ignores minor differences in the electric field distribution including fringe coupling that occurs at the ends of these segments, this method still serves as a valid first-order approximation because fringe coupling is not the dominant contributor to the FSS's impedance.

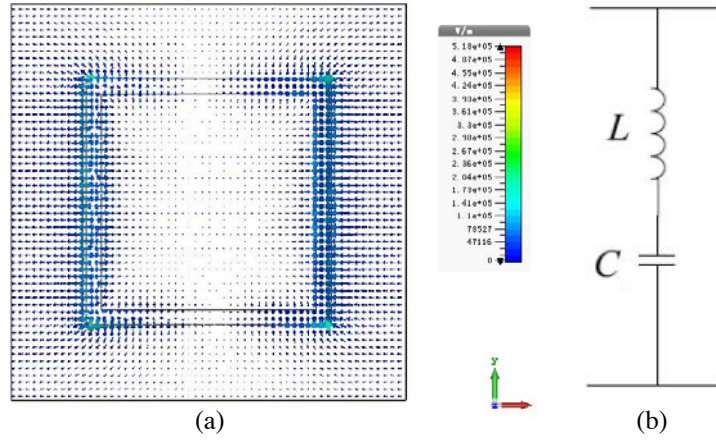


Figure 2. (a) Electric field distribution between adjacent elements for the loop FSS and (b) equivalent circuit model.

Using this conformal mapping approach, the response of the square-loop FSS to layered dielectrics can be determined. $\varepsilon_{r,eff}$ is related to how multiple surrounding dielectrics alter the impedance of an FSS, which is subsequently used to scale the wavelength in the FSS's inductance/capacitance approximation equations. Determining $\varepsilon_{r,eff}$ in this manner reduces the computation time (relative to a full-wave simulation). Additionally, this approach can aid the FSS design process by approximating how the frequency response of the FSS changes when it is embedded into a dielectric structure.

The conformal mapping involves a series of coordinate transformations to model the vertical cross

section of the square loop as a parallel-plate capacitance. For this dielectric structure, the total capacitance, C_t (from which $\epsilon_{r,eff}$ is calculated), of the FSS can be decomposed into a set of partial capacitances, which is described by $C_t = C_0 + C_1 + C_2 + C_3$, where C_0 is the capacitance of the coplanar strips in free space and C_1 , C_2 and C_3 are the capacitances resulting from the presence of the dielectric layer. The free-space capacitance C_0 is calculated in (5) using elliptic integrals of the first kind (denoted by K) that results from the conformal mapping transformation discussed in [8].

$$C_0 = \epsilon_0 \frac{K(k_0)}{K(k'_0)} \tag{5}$$

The values of variables k_0 and k'_0 are calculated using (6) and (7), respectively, which are dependent on the geometry of the coplanar strips, where w and g are defined above and are shown in Fig. 1.

$$k_0 = \sqrt{1 - \left(\frac{g}{w+g}\right)^2} \tag{6}$$

$$k'_0 = \sqrt{1 - k_0^2} \tag{7}$$

The capacitance C_n can be calculated as a set of equivalent dielectric layers using Eq. (8). ϵ_{rn} is the permittivity of layer n , and $\epsilon_{r(n+1)}$ is the permittivity of the next layer away from the FSS. h_n is the thickness between layer n and the FSS (including the thickness of layer n).

$$C_n = \frac{1}{2} (\epsilon_{rn} - \epsilon_{r(n+1)}) \frac{K(k)K(k'_n)}{K(k')K(k_n)} \tag{8}$$

$$K_n = \sqrt{1 - \frac{\sinh^2\left(\frac{\pi g}{2h_n}\right)}{\sinh^2\left(\frac{\pi(g+w)}{2h_n}\right)}} \tag{9}$$

$$K'_n = \sqrt{1 - K_n^2} \tag{10}$$

The total values of the FSS parameters are set as follows: $w1 = 0.1$ mm, $g1 = 1.7$ mm, $w2 = 0.17$ mm, and $g2 = 1.7$ mm, and the FSS structure is embedded between two dielectric sheets of Taconic TLY substrate with a permittivity of 2.2 and loss tangent of 0.0009. For the design in Fig. 3, $\epsilon_{r,eff}$ is calculated using Eq. (11) which takes the total capacitance C_t by C_0 . Using this conformal map, the values of $\epsilon_{r,eff}$ for the square-loop FSS are found to be 1.4461 and 1.4246 for the upper and lower FSS, respectively.

$$\epsilon_{reff} = 1 + \frac{1}{2}(\epsilon_{r1} - 1) \frac{K(k)K(k'_1)}{K(k')K(k_1)} + \frac{1}{2}(\epsilon_{r2} - \epsilon_{r3}) \frac{K(k)K(k'_2)}{K(k')K(k_2)} + \frac{1}{2}(\epsilon_{r3} - 1) \frac{K(k)K(k'_3)}{K(k')K(k_3)} \tag{11}$$

Next we use $\epsilon_{r,eff}$ to scale the wavelength in the FSS's inductance/capacitance approximation equations and obtain the reflection response of the whole structure. In Fig. 4, the S -parameters obtained using the conformal map are compared with the S -parameters obtained from the simulation performed using CST. Fig. 4(b) shows that the frequency response is extremely mismatched without depending on $\epsilon_{r,eff}$. In contrast, as shown in Fig. 4(a), the simulation and analytic results match well. The

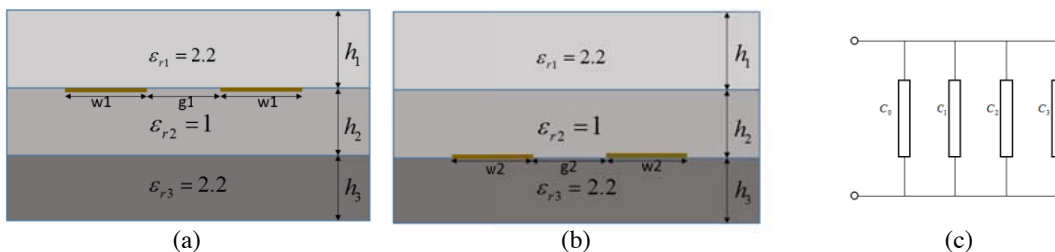


Figure 3. Single-square-loop FSS schematic: (a) top FSS, (b) bottom FSS, and (c) equivalent model.

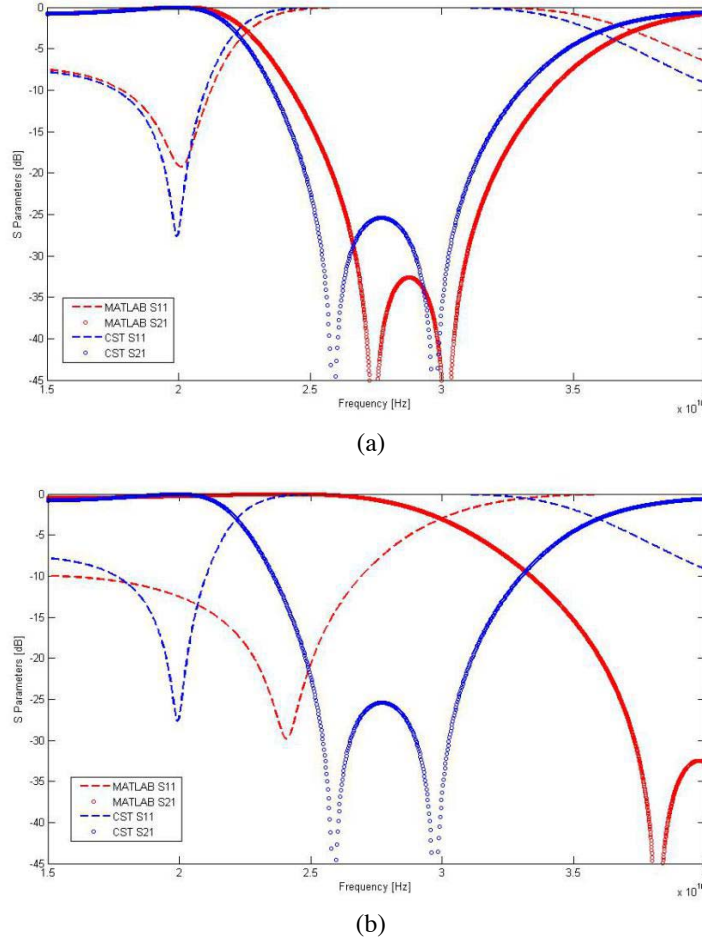


Figure 4. S_{11} and S_{21} amplitudes of the FSS (a) using $\epsilon_{r,eff}$ and (b) without using $\epsilon_{r,eff}$.

difference between the results is likely caused by inaccuracies in the impedance calculation performed using Marcuvitz's equations. As noted, the resonant depth generated by the CST simulation is deeper than that generated by the MATLAB program, which is largely because of the lack of coupling between the two FSSs in the MATLAB model (causing a decrease in the resonant depth). However, despite this limitation, the high computational speed (a few seconds, compared with the full-wave simulation, which often takes minutes) of this model indicates that it is a powerful analysis tool.

4. REFLECTARRAY DESIGN

After adjusting the FSS which exhibits appropriate performance, the suppressed mutual coupling feature indicates that the reflection characteristics can be controlled at each frequency band. In Fig. 5, a flowchart of the full design used in this reflectarray is presented. In the first stage, once the array has been configured, we obtain the required phase at each location. The S -parameter is also analyzed by simulation. Next, we build all elements in the array that are different from each other. To reduce the model-building time, a co-simulation approach is proposed in the design program. We use MATLAB to generate a VBScript to control the CST model, based on which the 3D model can be built and then solved automatically. The co-simulation approach not only decreases the amount of time required to design a model but also connects the optimization and verification operations.

Taking the FSS structure into account in the unit cell model, the optimized double-ring unit based on the variable-size technique is used at 30 GHz, and a conventional double-ring unit with a metal back is used at 20 GHz. One of these double-ring cells is depicted in Fig. 1. The adjusted parameters for

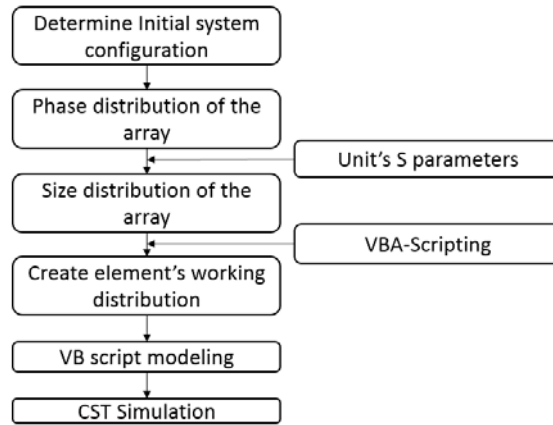


Figure 5. Flowchart of the full design.

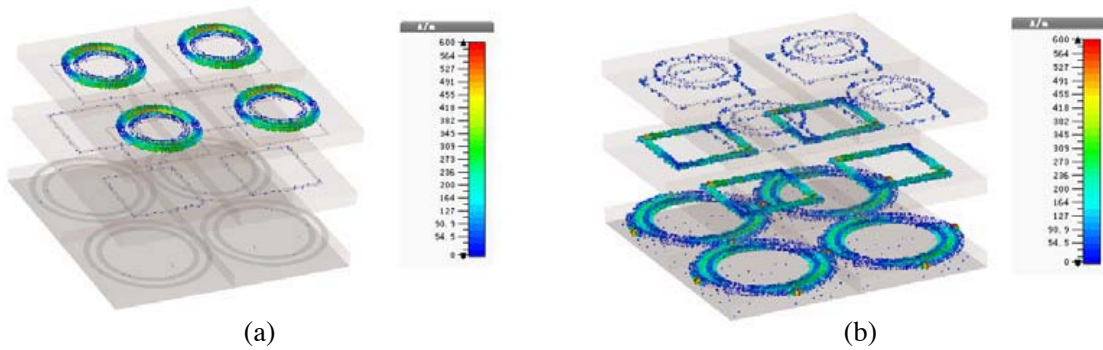


Figure 6. Current distribution of the unit (a) at 30 GHz and (b) at 20 GHz.

the cell are $r_{u2} = 0.7 * r_{u1}$ and $r_{d2} = 0.8 * r_{d1}$, with the double-ring elements lying on the substrate layer. The dimensions of the double-ring unit (r_{u1} varies from 2 mm to 3.5 mm, and r_{d1} varies from 2.5 mm to 4.5 mm) account for the phase shift. The periodic structure is arranged in a square lattice with $P = 4.5$ mm.

An infinite periodic model using CST simulation is performed to analyze the reflection and transmission characteristics. In Fig. 6, the current distribution density of the element is shown for both bands. We observe that the current at 30 GHz occurs only in the upper element. The bottom element does not account for the radiation characteristics. It should be noted from Fig. 6(b) that the current distribution on the upper element is much weaker than that on the bottom element; thus the incident wave can mostly be transmitted through FSS at 20 GHz and finally generates resonance at the bottom unit. As expected, the incident wave is mostly transmitted at 20 GHz and reflected at 30 GHz in the FSS, which means that the unit can be excited effectively to realize the radiation pattern.

Sweeping the phase parameter R_{u1} from 2 to 3.5 mm in steps of 0.075 mm and the phase parameter R_{d1} from 2.5 to 4.5 mm in steps of 0.1 mm independently, two-dimensional reflection phase and magnitude can be obtained, as shown in Fig. 7 and Fig. 8. Fig. 7 clearly shows that 360° phase variation at both 20 GHz and 30 GHz can be achieved linearly. When the size of the 20-GHz element is changed, the 30-GHz phase change is left intact; at 20 GHz, changes in 30-GHz element alter, to some extent, the phase-shift provided by R_d , especially for the lower values of R_u . Once the required phase shift is determined at 30 GHz, the phase shift at 20 GHz can be selected in the data table according to Figs. 7 and 8. The simulated amplitude properties are shown in Fig. 8(b): the element loss for both bands decreases drastically, with maximum losses of 0.2 dB at 20 GHz and 0.1 dB at 30 GHz, demonstrating that this double-ring structure can scatter only the desired frequency and is transparent

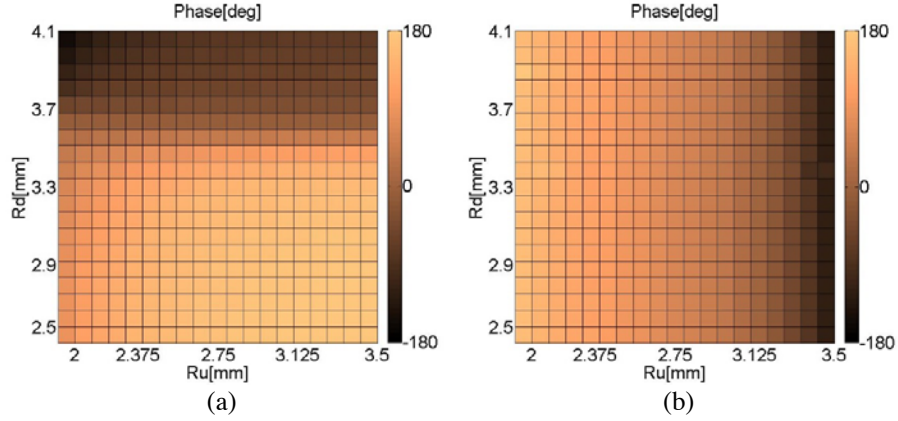


Figure 7. Phase at (a) 20 GHz and (b) 30 GHz.

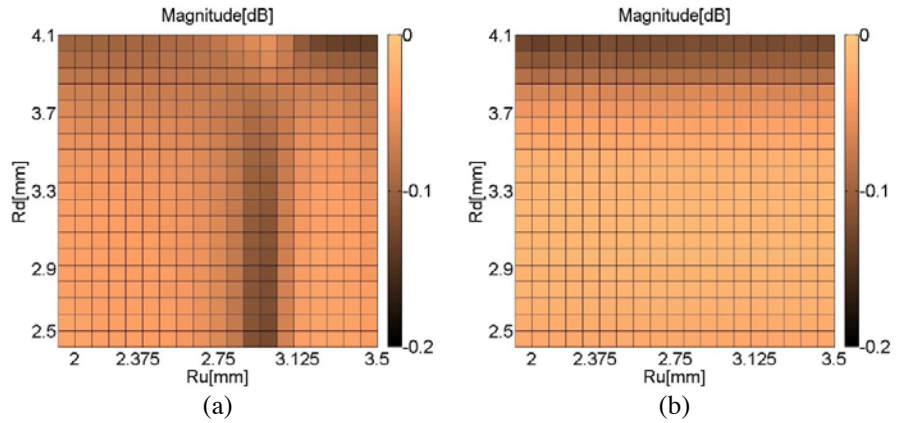


Figure 8. Amplitude at (a) 20 GHz, (b) 30 GHz.

to electromagnetic waves with other frequencies.

The reflectarray antenna is designed to collimate a pencil beam in the specular direction, $\phi = 180^\circ$ and $\theta = 30^\circ$, at both 20 GHz and 30 GHz; this configuration is used to minimize feed blockage from the horn located 85 mm from the aperture. The configuration is summarized in Table 1. Due to the unit cell spacing of 4.5 mm, 20×20 cells are selected. Because of the symmetry of the reflectarray plate, it is possible to use a magnetic symmetry plane.

Table 1.

RX frequency	19.7 GHz \sim 20.2 GHz
TX frequency	29.5 GHz \sim 30.0 GHz
Aperture dimensions	90 mm \times 90 mm ($6\lambda_d$ at 20 GHz and $9\lambda_u$ at 30 GHz)
Feed distance to the aperture	85 mm
Feed angle	$\phi = 0^\circ$ $\theta = 0^\circ$
Beam angle	$\phi = 180^\circ$ $\theta = 30^\circ$

The circularly polarized reflectarray is illuminated by two separate circular corrugated horns: one for 20 GHz and the other for 30 GHz. The corresponding gains are equal to 14.1 dBi at both frequencies. The f/D ratio of the RA is 0.72, which provides proper illumination with a 9.29-dB edge taper and maximizes the aperture efficiency. To simplify the simulation and decrease the number of resources

required for the simulation, the feed antenna is center-fed, but the main beam is oriented near 30° to mitigate feed blockage. A preliminary numerical analysis of the unit shows that the effect of the mutual coupling between the two bands can be neglected; therefore, the dual-frequency reflectarray design is simplified to two single-frequency reflectarray designs. The required compensating phase shift for each element is determined using ray tracing, as shown in Fig. 9. When the reflectarray antenna design is complete, there are two full-wave simulation models for each band: one is the complete antenna configuration, including the FSS structure, and the other is the configuration with the FSS.

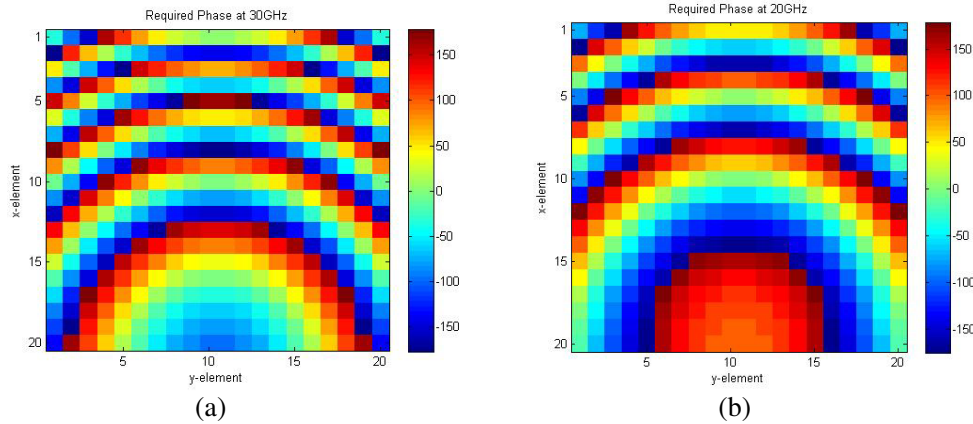


Figure 9. Phase shift on reflectarray aperture: (a) 30 GHz and (b) 20 GHz.

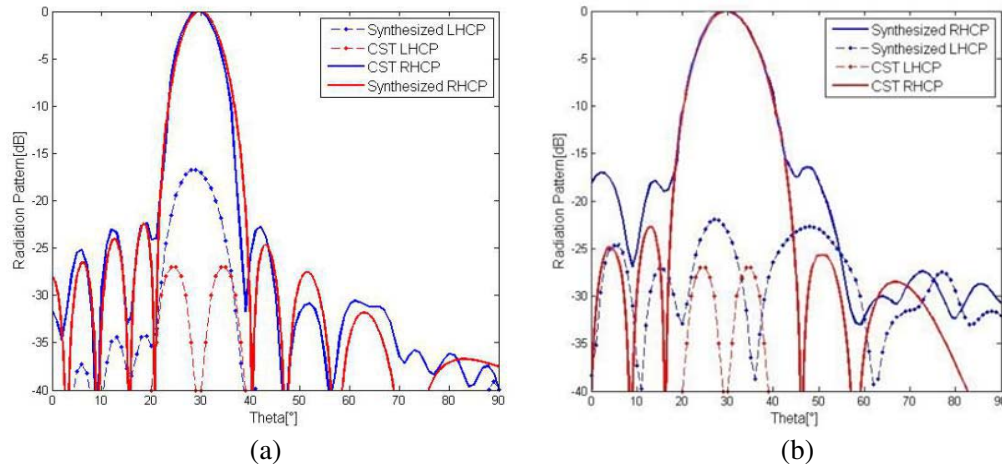


Figure 10. Synthesized and simulated radiation patterns: (a) 30 GHz and (b) 20 GHz.

Because the analytical method introduced above exhibits the advantage of easy optimization, the proposed reflectarray can be designed according to the working frequency. The proposed reflectarray antenna is simulated using CST; the simulated co- and cross-polarizations at 20 GHz and 30 GHz are shown in Fig. 10. The simulated gain is 27.7 dB at 30 GHz with side-lobe levels of -19.3 dB. The simulated cross-polarization level is less than -25.2 dB. Fig. 10(b) depicts the simulated radiation patterns of the antenna at 20 GHz with a gain of 23.3 dB and side-lobe levels of -17 dB. The simulated cross-polarization levels are less than -23 dB. Fig. 11 shows the simulated gain as a function of the frequency for both reflectarrays. The 1-dB gain bandwidths at 30 GHz and 20 GHz are 6.67% and 8.76%, respectively. The aperture efficiency ε is calculated using $\varepsilon = G_m/D_{ideal}$, where G_m is the simulated gain, D_{ideal} the ideal directivity given by $D_{ideal} = 4\pi A/\lambda_0^2$, A the aperture area of the antenna, and λ_0 the free-space wavelength. The aperture efficiency of the reflectarray antenna is 57.85% at 30 GHz and

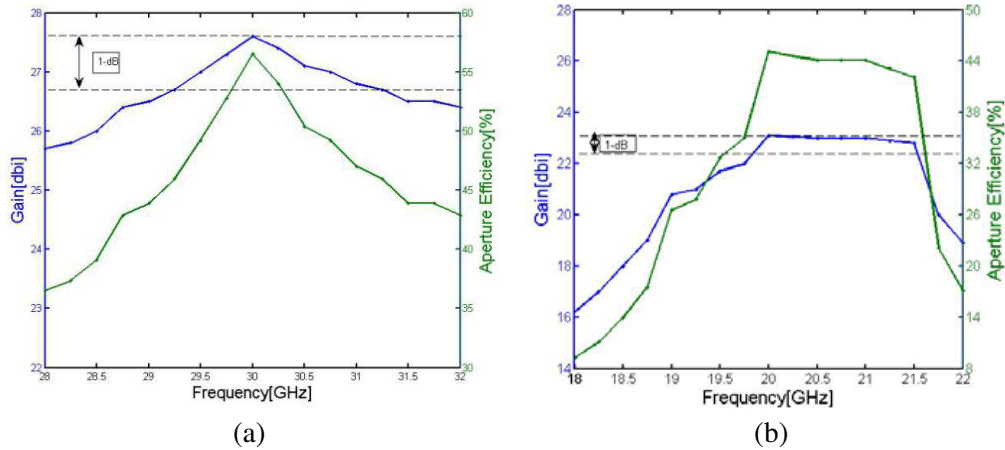


Figure 11. Simulated gain and efficiency: (a) 30 GHz and (b) 20 GHz.

47.25% at 20 GHz.

There are different ways to design dual-band reflectarrays. Most of the configurations are implemented by exploiting multiple layers, and some are realized by a single-layer structure. To simplify this multilayer configuration, a broadband FSS in a single layer instead of two layers FSS in this paper could be considered to release the complexity of the whole structure. In this case, designing an FSS with a wide and flat bandpass frequency response will be the key issue. The frequency response of FSS in arbitrary layered dielectric structures can also be calculated by conformal mapping.

5. CONCLUSIONS

This paper presents a novel circularly polarized dual-band reflectarray antenna. Conformal mapping is used to estimate the effective permittivity ($\epsilon_{r,eff}$) of a square-loop FSS embedded into the dielectric structure of the dual-band reflectarray antenna, which can rapidly synthesize the frequency response of this antenna model. This technique significantly simplifies the antenna design process, and the mutual coupling of the receiving and transmitting bands is suppressed. This reflectarray antenna with an aperture of 90 mm operates at 30 GHz and 20 GHz with 57.85% and 47.25% aperture efficiencies, respectively. Moreover, the 1-dB gain bandwidths of the 30- and 20-GHz bands are 6.67% and 8.76%, respectively. The good agreement between the numerical analysis and simulated results demonstrates the freedom to control the radiated beam in each band separately.

ACKNOWLEDGMENT

This work was supported by the National Natural Science Foundation of China under grant No. 11475182.

REFERENCES

1. Shaker, J. and M. Cuhaci, "Multi-band, multi-polarization reflector reflectarray antenna with simplified feed system and mutually independent radiation pattern," *IEE Proceedings — Microwaves Antennas and Propagation*, Vol. 152, No. 2, 97–101, 2005.
2. Chaharmir, M. R. and J. Shaker, "Design of an FSS-backed 20/30 GHz circularly polarized reflectarray for shared aperture X/Ka-band satellite applications," *International Symposium on Antenna Technology and Applied Electromagnetics*, 1–1, IEEE, 2014.

3. Smith, T., U. Gothelf, O. S. Kim, and O. Breinbjerg, "Design, manufacturing, and testing of a 20/30-GHz dual-band circularly polarized reflectarray antenna," *IEEE Antennas Wireless Propag. Lett.*, Vol. 12, 1480–1483, Nov. 2013.
4. Shaker, J., M. R. Chaharmir, and H. Legay, "Investigation of FSS-backed reflectarray using different classes of cell elements," *IEEE Transactions on Antennas and Propagation*, Vol. 56, No. 12, 3700–3706, Dec. 2008.
5. Chaharmir, M. R. and J. Shaker, "Design of an FSS-backed 20/30 GHz circularly polarized reflectarray for shared aperture X/Ka-band satellite applications," *International Symposium on Antenna Technology and Applied Electromagnetics*, 1–1, IEEE, 2014.
6. Deng, R., F. Yang, S. Xu, et al., "An FSS-Backed 20/30 GHz dual-band circularly polarized reflectarray with suppressed mutual coupling and enhanced performance," *IEEE Transactions on Antennas and Propagation*, Vol. PP, No. 99, 1–1, 2017.
7. Schinzinger, R. and P. A. A. Laura, *Conformal Mapping: Methods and Applications*, Dover Publications Inc., Mineola, New York, 1991.
8. Chen, E. and S. Chou, "Characteristics of coplanar transmission lines on multilayer substrates: modeling and experiments," *IEEE Trans. Microwave Theory Tech.*, Vol. 45, No. 6, 939–945, Jun. 1997.
9. Marcuvitz, N., *Waveguide Handbook*, McGraw-Hill, New York, 1951.